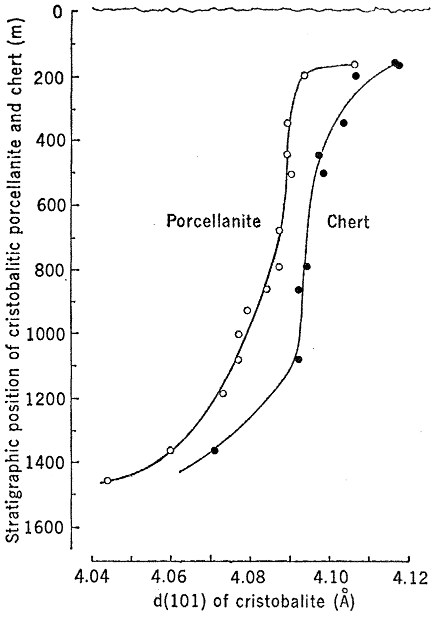

Fig. 2. Variation with depth of the $d(101)$ spacing of cristobalite in porcellanite (open circles) and chert (closed circles) at Chico Martinez Creek. Depths are relative to the top of the Monterey Shale and represent minimal depths of burial.

Another and earlier diagenetic stage is represented higher in the section, where there are alternating layers of chert and diatomaceous mudstone; only the chert is cristobalitic, and free silica of the associated mudstone consists of unaltered biogenic opal (diatom frustules) that is amorphous to x-rays. The final diagenetic stage is found at other localities, where chert and porcellanite in the lower part of the Monterey are both quartzitic.

Our observations suggest that the alteration of biogenic opal occurred first in layers of purest diatomite through dissolution of diatom frustules and precipitation of cryptocrystalline cristobalite. These layers, which originally had a density of about 0.5 g/cm^3, also served as loci of deposition for some silica dissolved out of adjacent diatomaceous mudstone and were gradually converted into compact cristobalitic chert with a density of about 2.0 g/cm^3. The change of diatomaceous mudstone into cristobalitic porcellanite occurred some time afterwards (*4*, p. 54). The ratio of chert to porcellanite in the exposure of Fig. 1 is believed to reflect approximately the ratio of diatomite to diatomaceous mudstone in the original sediment.

Cristobalitic porcellanite is a dominant type of rock in the Monterey Shale at many places. At the classic Miocene locality of Chico Martinez Creek in western Kern County (*5*), there is about 1300 m of cristobalitic porcellanite accompanied by variable amounts of cristobalitic chert. Below the cristobalitic diagenetic zone, porcellanite and chert in an additional 730 m of Monterey Shale are uniformly quartzitic.

Diagenetic cristobalite of the Monterey Shale manifests an increasing sharpness of x-ray reflections and a decreasing $d(101)$ spacing in successively older samples that represent increasing depth of burial. Such changes in response to x-rays have been ascribed (*6*) to a progressive ordering of the disordered atomic structure of the first-formed cristobalite, which is favored by increasing temperature and pressure. Cristobalitic porcellanite and chert of Chico Martinez Creek (and of other California localities as well) unexpectedly have separate curves relating their $d(101)$ spacing to depth of burial (Fig. 2). At any particular horizon, the spacing of porcellanite is 0.004 to 0.015 Å smaller than that of associated chert, probably because porcellanite formed later (at a higher temperature) than the chert.

The total variation of $d(101)$ spacing of cristobalite in the Monterey Shale is 4.040 to 4.115 Å, with a standard deviation of determination of 0.0026 Å. The numerical value of the spacing in angstroms seems to be a useful index of structural state, and a notation such as Cr(4.110), Cr(4.085), and Cr(4.050) could be substituted for the qualitative terms disordered, partly ordered, and ordered in describing diagenetic cristobalite. The porcellanite in Fig. 1 is Cr(4.103), the chert, Cr(4.107). Precise characterization of cristobalite would add welcome detail to an important stage in the diagenesis of siliceous shales.

K. J. MURATA
J. K. NAKATA

U.S. Geological Survey,
Menlo Park, California 94025

References

1. S. E. Calvert, *Contrib. Mineral. Petrol.* **33**, 273 (1971).
2. G. R. Heath and R. Moberly, Jr., in *Initial Reports of the Deep Sea Drilling Project* (Government Printing Office, Washington, D.C., 1971), vol. 7, p. 914; W. H. Berger and U. von Rad, in *ibid.* (1972), vol. 14, p. 787; R. Greenwood, *J. Sediment. Petrol.* **43**, 700 (1973); S. W. Wise, Jr., B. F. Buie, F. M. Weaver, *Eclogae Geol. Helv.* **65**, 157 (1972).
3. K. J. Murata, I. Friedman, M. Cremer, *U.S. Geol. Surv. Prof. Pap. 724-C* (1972).
4. M. N. Bramlette, *U.S. Geol. Surv. Prof. Pap. 212* (1946).
5. T. W. Dibblee, Jr., *U.S. Geol. Surv. Prof. Pap. 764* (1973).
6. O. W. Floerke, *Neues Jahrb. Mineral. Monatsh.* **10**, 217 (1955); W. Eitel, *Geol. Soc. Am. Spec. Pap. 66* (1958); C. Frondel, *The System of Mineralogy of James Dwight Dana and Edward Salisbury Dana, Yale University, 1837–1892* (Wiley, New York, ed. 7, 1962), vol. 3, pp. 273–286; J. B. Jones and E. R. Segnit, *J. Geol. Soc. Aust.* **18**, 57 (1971).

19 December 1973

■

Nitric Oxide Reduction Coupled with Carbon Monoxide Oxidation in the Presence of Soluble Metal Catalysts

Abstract. *Solutions of* $RhCl_3 \cdot xH_2O$ *in ethanol and* $Ru(NO)_2[P(C_6H_5)_3]_2$ *in benzene catalyze the reduction of nitric oxide to nitrous oxide concomitant with the oxidation of carbon monoxide to carbon dioxide at ambient temperature and atmospheric pressure. The reaction, which is followed by gas chromatography and by the decrease in pressure of the system, proceeds to 47 percent conversion of the reactants after 63 hours.*

Oxides of nitrogen, NO_x, comprise an important environmental problem, and this has led to increased study of the reactions of the parent member of this series, nitric oxide. The decomposition of nitric oxide to the elements has been known and studied for years by using noble metal and metal oxide catalysts at high temperatures (*1*). However, this decomposition also leads to the formation of NO_2 by the rapid reaction $NO + \frac{1}{2}O_2 \rightarrow NO_2$. A more promising approach has been to reduce NO by using CO, H_2, or NH_3 as reductants with the aid of noble metal, copper oxide, or rare earth manganite catalyst systems (*2*). Temperatures for these reactions are generally in excess of 200°C. We now report that the coupled reaction of NO reduction and CO oxidation proceeds readily at ambient temperature and atmospheric pressure in the presence of soluble metal complexes to yield N_2O and CO_2. Moreover, this coupled reaction is catalytic in metal complex.

Catalyst solutions employed in this study include $RhCl_3 \cdot xH_2O$ in ethanol and $Ru(NO)_2(PPh_3)_2$ (where $Ph = C_6H_5$) in benzene. In a typical experiment, 0.1 to 1.0 mmole of metal complex is dissolved in 50 ml of solvent and the solution is placed in an apparatus composed of a 250-ml flask connected to a 1-liter gas mixing bulb attached to a manometer. The system is degassed and evacuated to an initial pressure corresponding to the solvent vapor pressure at room temperature (23°C). A gas mixture of NO and CO (2 : 1) is then added to the system until a system pressure between 710 and 760 mm is obtained, and the solution is well stirred. The gases in the system are sampled periodically by gas chromatography. For this purpose two columns are employed: the first, molecular sieve 5-A, allows separation of the diatomic gases N_2, O_2, CO, and NO, while the second, Poropak Q, permits observation of the product gases CO_2 and N_2O distinct from the initial gases in the system.

Standard samples of all gases were chromatographed, as were mixtures of the gases, to verify retention times and allow estimates of relative concentrations. Blank systems composed of solvent plus the mixture of NO and CO gases were also used to show that the metal complexes are necessary for the coupled reaction.

Table 1 shows the estimated partial pressures of the reactant and product gases as a function of time for an experiment in which the catalyst solution was $RhCl_3 \cdot xH_2O$ in ethanol. Of the catalyst systems tested, this one appears to be most effective. The two major products are N_2O and CO_2. In addition, there is a possibility that small amounts of dinitrogen (N_2) are also formed, but this could not be established unequivocally because of the presence of traces of N_2 in the reactant gases, and the appearance of a consistently minor N_2 peak in the gas chromatographs.

Since the primary reaction observed was

$$2NO + CO \rightarrow N_2O + CO_2 \quad (1)$$

it was followed by the pressure decrease in the system as a function of time. The results are presented in Fig. 1 as a plot of total system pressure against time. The linearity of the plot between 15 and 30 hours indicates that the reaction is initially controlled solely by the catalyst concentration and is zeroth order in reactant gases. Verification of this is obtained when the catalyst concentration is varied and the rate of reaction changes correspondingly. Curvature in the plot presented in Fig. 1 develops after about 35 hours, when we estimate that 35 percent of the reactants have been converted to products. Variation of the relative NO and CO gas pressures to examine their rate dependence at this stage of the reaction remains to be studied. The reaction is greatly favored thermodynamically and should proceed to essential completion.

Table 1. Partial pressures (p) of reactant and product gases. The reactant gases were NO and CO. The catalyst used in this experiment was 1 mmole of $RhCl_3 \cdot xH_2O$ in 50 ml of ethanol. Pressures were estimated from calibration curves by use of gas chromatography; the estimated standard deviation for these values is 5 mm.

Time (hours)	p_{NO} (mm)	p_{CO} (mm)	p_{N_2O} (mm)	p_{CO_2} (mm)
3.5	476	257	16	7
16.1	455	215	36	36
20.3	440	205	39	41
28.0	397	182	52	55
39.0	360	168	63	70
50.5	329	150	80	86
63.3	293	138	92	99

Estimates of the percentage conversion of reactants based on Fig. 1 have been supported by gas sampling studies which show that after 28 and 63 hours, respectively, 24 and 47 percent of the reactant gases have been consumed. As yet no attempts have been made to increase the reaction rate by increasing the temperature above 23°C or by increasing the efficiency of gas-solution mixing.

The initial static pressure in the system can be ascribed to a number of factors. First is the slow mixing of the gases at the surface of the reaction solution resulting from a constriction between the 250-ml flask and the 1-liter gas mixing bulb (the gases were not premixed). Second and most important is an induction period in which the catalytically active species is formed. Other catalytic studies employing $RhCl_3 \cdot xH_2O$ have also shown induction periods (*3*). In the reaction described here, the solution changes in color from red-brown to brown, and eventually green or yellow in more dilute solutions. The reaction does not begin until the initial color change. Thus, the exact nature of the catalytically active species in solution is of importance.

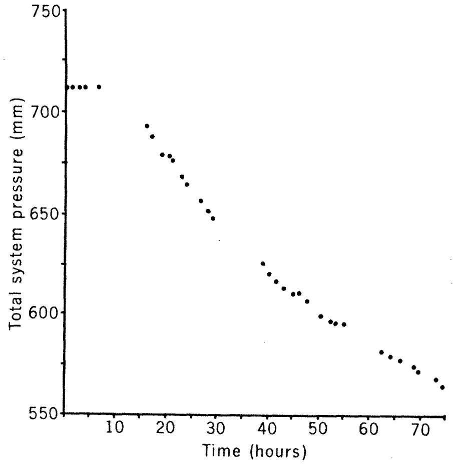

Fig. 1. A plot of total pressure against time for a mixture of NO and CO gases (2 : 1) in a system containing 1 mmole of $RhCl_3 \cdot H_2O$ in 50 ml of ethanol as catalyst. Each measurement is ± 2 mm.

Conversion of NO to N_2O and CO to CO_2 is also observed, but is slower, when $Ru(NO)_2(PPh_3)_2$ in benzene is used as the catalyst solution. In this system the phosphine ligands may block the coordination sites needed for the reaction to proceed quickly. Initially, it was thought that the presence of added phosphine would lead to greater amounts of N_2 with the concomitant formation of triphenylphosphine oxide, but this is not borne out by experiment.

The fact that $RhCl_3$ solutions catalyze coupled NO reduction and CO oxidation is, in retrospect, not surprising. The reaction of Rh(I) complexes with NO to yield Rh(III) plus N_2O has been reported (*4*), as has the reduction of Rh(III) by CO to give Rh(I) and CO_2 (*5*). However, the coupling of these two reactions with soluble metal complexes as catalysts is new, and the mild conditions under which it occurs are striking.

Such coupling of reactions with soluble metal catalysts may have important implications. First, these reactions may help elucidate the reactivity of coordinated NO and the mechanism of its decomposition, and thus lead to a more rational approach in the design of commercial catalyst systems. Second, the idea of coupled reactions with metal complexes can be extended to other systems, most notably CO oxidation with SO_2 reduction. It thus appears that "molecular handles" for these intriguing reactions, which have been reported before in heterogeneous catalyst systems (*1*), may finally be at hand.

JOSEPH REED
RICHARD EISENBERG

Department of Chemistry,
University of Rochester,
Rochester, New York 14627

References and Notes

1. T. E. Green and C. N. Hinshelwood, *J. Chem. Soc. (Lond.)* (1926), p. 1709; C. S. Howard and F. Daniels, *J. Phys. Chem.* **62**, 360 (1958); J. M. Fraser and F. Daniels, *ibid.*, p. 215; E. R. S. Winter, *J. Catal.* **22**, 158 (1971); M. Shelef, K. Otto, H. Ghandi, *Atmos. Environ.* **3**, 107 (1969); S. W. Harris, E. F. Morello, G. H. Peters, U.S. Patent No. 3,459,494.
2. P. R. Ryason and J. Harkins, *J. Air Pollut. Control Assoc.* **17**, 796 (1967); H. C. Andersen, W. J. Green, D. R. Steele, *Ind. Eng. Chem.* **53**, 199 (1971); K. Otto and M. Shelef, *J. Phys. Chem.* **76**, 37 (1972); R. J. H. Voorhoeve, J. P. Remeika, D. W. Johnson, Jr., *Science* **180**, 62 (1973); J. Cohn, D. R. Steele, H. C. Anderson, U.S. Patent No. 2,975,025.
3. R. Cramer, *J. Am. Chem. Soc.* **87**, 4717 (1965).
4. W. B. Hughes, *Chem. Commun.* (1969), p. 1126.
5. B. R. James and G. L. Rempel, *ibid.* (1967), p. 158.
6. Supported by NSF grant GP-40088X. R.E. is an Alfred P. Sloan Foundation Fellow, 1972 to 1974.

8 January 1974

■

Air Pollution: Remote Detection of Several Pollutant Gases with a Laser Heterodyne Radiometer

Abstract. *An infrared heterodyne radiometer with a spectral resolution of 0.04 reciprocal centimeters has been used to remotely detect samples of ozone, sulfur dioxide, ammonia, and ethylene at room temperature, and samples of nitric oxide at 390K. Each gas was observed in a background of nitrogen or oxygen at atmospheric pressure. Sensitivities to some of these gases are adequate for detection of ambient concentrations as low as a few parts per billion.*

A heterodyne radiometer, with a CO_2 laser as a local oscillator, has been used to remotely detect several laboratory samples of gaseous pollutants at ambient temperature. The radiometer is a passive device, sensitive to the characteristic thermal radiation from each gas. Previous demonstrations of heterodyne radiometer sensitivities to SO_2 and CO_2 were accomplished by heating the gas samples (*1*). The sensitivities to O_3, NH_3, and CH_4 were found to be adequate for detection of ambient concentrations in the parts per billion (ppb) region. The sensitivities to SO_2 are on the border line for detection of ambient concentrations around 50 ppb, and it may be possible to improve this by a factor of 4 if detection wavelengths near 8.8 μm are used instead of our operating region around 9.0 μm. A CO laser, operating near 5.2 μm, has also been used as a local oscillator in the detection of nitric oxide (NO) at a temperature of 390 K. The passive heterodyne radiometer does not appear to be capable of detecting ambient NO at normal smog concentrations; however, it can be used to monitor NO concentrations in stationary source emissions which are at elevated temperatures.

The heterodyne radiometer is useful for remote observation and measurement of atmospheric constituents whenever high spectral resolution is desired. The spectral resolution makes the instrument very selective, as interference problems due to overlapping lines or bands are minimized. Possible applications include monitoring of local air pollution from the ground or of global atmospheric quality from spacecraft. There are also several applications in infrared astronomy. Applications to remote sensing of atmospheric pollutants have been discussed in connection with infrared tunable diode lasers (*2*) and infrared gas lasers (*3*).

The heart of the instrument consists of an infrared laser as a local oscillator, and a high-speed infrared detector. The local oscillator beam and the radiation to be detected are normally combined via a beam splitter and are then focused onto the detector, which acts as a mixer. The instrument is sensitive to a narrow (by infrared standards) band of beat frequencies on each side of the local oscillator frequency. The sensitive bandwidth is determined by the frequency responses of the infrared detector and the intermediate frequency (IF) amplification chain which follows the detector. Since the size of the mixing signal increases as the local oscillator power increases, the ultimate sensitivity is reached when local oscillator fluctuations become the chief source of noise. If a Dicke-type radiometer configuration is used, and the only local oscillator fluctuations are due to quantum fluctuations, then the signal-to-noise ratio (S/N) when the radiometer is looking at a radiating slab of gas at temperature T with emissivity $\varepsilon(\nu)$ is

$$\frac{S}{N}=\frac{1}{4}\,\frac{\eta\,(\tau/B)^{1/2}}{\exp\left(\frac{h\nu}{kT}\right)-1}\int_{\nu_{\mathrm{LO}}-B}^{\nu_{\mathrm{LO}}+B}\epsilon(\nu)d\nu \qquad (1)$$

(*1*). In this expression η is the quantum efficiency of the infrared mixer (about 0.5 in our case), ν_{LO} is the local oscillator frequency, B is the IF bandwidth, and τ is the integration time after the IF detection process. In practice, the frequencies of IF amplification range from a few to several hundred megahertz. Thus, the integration range in Eq. 1 is not strictly correct, but it is a good approximation.

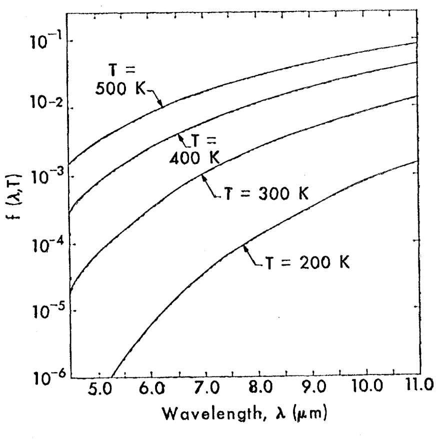

Fig. 1. Wavelength dependence of the sensitivity of the heterodyne radiometer. The function plotted is $f(\lambda, T) = [\exp(hc/\lambda kT) - 1]^{-1}$; $\nu = c/\lambda$ where c is the velocity of light. (See Eq. 1 in text.) The temperatures indicated here are those of the gases within the radiometer's field of view.

Although the frequency-dependent expression $[\exp(h\nu/kT)-1]^{-1}$ in Eq. 1 varies slowly enough to be placed outside the integral, it produces a large effect in values of S/N for radiometer operation at various infrared wavelengths. As we see in Fig. 1, this causes the heterodyne radiometer to be much more sensitive to radiating gases when operating at longer wavelengths in the infrared. Thus, at room temperature the sensitivity to gases that radiate in the wavelength region above 9 μm is much better than the sensitivity to NO, which radiates in the region from 5.0 to 5.5 μm.

In our experiments, a CO_2 laser was used to provide emission frequencies which overlapped emission lines of SO_2, O_3, C_2H_4, and NH_3. A CO laser, cooled with a Dry Ice–methanol closed cycle system, was used to provide a local oscillator line which overlapped an NO emission line. Both lasers were sealed off and had very stable frequencies. Each laser could be tuned over a large number of lines by adjusting a diffraction grating at one end of the cavity. Sodium chloride optics were used to combine the local oscillator and thermal radiation signals, and focus them onto a high-speed germanium photoconductor doped with copper. The mixer was roughly 0.3 by 0.4 by 3.5 mm. The cross-sectional dimensions were made small in order to reduce the capacitance and operating resistance of